Supplementary Information File for "Ring-Polymer Molecular Dynamics for the Prediction of Low-Temperature Rates: An Investigation of the C(^{1}D) + H_2 Reaction"

Kevin M. Hickson,* Jean-Christophe Loison, Hua Guo, and Yury V. Suleimanov*

E-mail: km.hickson@ism.u-bordeaux1.fr; ysuleyma@mit.edu

Experimental Methodology

Three different Laval nozzles were employed in this study allowing measurements to be performed at 50 K, 75 K and 127 K. Room temperature experiments were performed by removing the nozzle, thereby using the apparatus as a slow-flow reactor. The temperature, density and velocity of the supersonic flows were calculated from separate measurements of the impact pressure within the supersonic flow and the stagnation pressure within the reservoir. The measured and calculated values are summarized in Table S2 alongside other relevant information.

One potential source of error in the experiments is the possibility that non-reactive quenching collisions between C(^{1}D) and H_2 could lead to an overestimate of the reactive rate coefficient. As non-reactive collisions should lead to less atomic hydrogen formation as the H_2 concentration increases, tests were performed at 127 K in which kinetic traces for H atom formation were recorded sequentially at three different H_2 concentrations, thus allowing us to compare the H atom signal amplitudes as a function of time. The procedure was repeated several times, varying the order of the different [H_2] to correct for potential signal drift over the timescale of the experiment. The peak H atom signal intensities for each [H_2] were then averaged and compared.

Rather than observing a decrease in the H atom signal intensity with increasing [H_2], which is the effect that should be observed if quenching collisions are important, we saw instead that the average peak H atom signal recorded with lower [H_2] were lower than the high [H_2] one. This effect can be explained by taking in to consideration the diffusional loss of C(^{1}D) over the same time period. For the high [H_2] measurements (with [H_2] = 3.4 $\times$ 10^{14} cm^{-3}), the C(^{1}D) reacts rapidly (the peak signal occurs around 22 μs), leading to low diffusional losses and a correspondingly large H atom signal amplitude. Conversely, for lower [H_2] measurements (with [H_2] = 1.7 $\times$ 10^{14} cm^{-3} and 7.0 $\times$ 10^{13} cm^{-3}), the C(^{1}D) atoms have more time to diffuse from the observation zone (the peak H atom signals for these [H_2] occurs at 32 μs and 56 μs respectively) leading to lower peak H atom signals.

Experimentally, after 32 μs reaction time, the average peak H atom signal represents 96% of the average signal at 22 μs. Similarly, after 56 μs, the average peak H atom signal was found to represent 89% of the signal at 22 μs. These values were compared with a simple simulation employing a diffusional loss value for C(^{1}D) of 3500 s^{-1} (our earlier measurements at 127 K of the C(^{3}P) + CH_3OH reaction under similar conditions [54] indicate that C(^{3}P) atoms were lost by diffusion with constants around 3500 s^{-1} from the y-intercept values of corresponding second-order plots). The simulations predict that 96 % and 90 % of the initial C(^{1}D) remains after 32 μs and 56 μs respectively when compared to the corresponding value at 22 μs; in good agreement with the experimental values. This result clearly indicates that non-reactive loss of C(^{1}D) through collisions with H_2 is negligible over the range of [H_2] used in the present experiments, so that the rate coefficients measured arise from reactive loss of C(^{1}D) with H_2. The measured rate coefficients are listed in Table II alongside other relevant information.

Table S1: Input parameters for the RPMD calculations on the C(^{1}D) + H_2. The explanation of the format of the input file can be found in the RPMDrate code manual (http://ysuleyma.scripts.mit.edu).

Parameter	Potential Energy Surface		Explanation
	$^1A'$	$^1A''$	
Command line parameters			
`Temp`	300		Temperature (K)
	128		
	77		
	50		
`Nbeads`	128(300 K); 196(77,128 K), 256(50 K)		Number of beads
Dividing surface parameters			
R_∞	20 a_0	20 Å	Dividing surface parameter (distance)
N_{bonds}	1	1	Number of forming and breaking bonds
N_{channel}	2	2	Number of equivalent product channels
C(^{1}D)	(1.635 a_0, 1.302 a_0, 0.000 a_0)	(-2.450 a_0, 0.000 a_0, 0.000 a_0)	Cartesian coordinates (x, y, z)
H	(0.000 a_0, 0.000 a_0, 0.000 a_0)	(0.000 a_0, 0.000 a_0, 0.000 a_0)	of the intermediate geometry
H	(3.270 a_0, 0.000 a_0, 0.000 a_0)	(1.900 a_0, 0.000 a_0, 0.000 a_0)	
`Thermostat`	'Andersen'	'Andersen'	Thermostat option
Biased sampling parameters			
N_{windows}	111	111	Number of windows
ξ_1	-0.05	-0.05	Center of the first window
$d\xi$	0.01	0.01	Window spacing step
ξ_N	1.05	1.05	Center of the last window
dt	0.0001	0.0001	Time step (ps)
k_i	2.72	2.72	Umbrella force constant ((T/K) eV)
$N_{\text{trajectory}}$	200	200	Number of trajectories
$t_{\text{equilibration}}$	20	20	Equilibration period (ps)
t_{sampling}	100	100	Sampling period in each trajectory (ps)
N_i	2×10^8	2×10^8	Total number of sampling points
Potential of mean force calculation			
ξ_0	0.00	0.00	Start of umbrella integration
$\xi^\ddagger$	0.599 (300 K)[a]	0.921 (300 K)[a]	End of umbrella integration
	0.445 (128 K)[a]	0.806 (128 K)[a]	
	0.393 (77 K)[a]	0.763 (77 K)[a]	
	0.359 (50 K)[a]	0.746 (50 K)[a]	
N_{bins}	5000	5000	Number of bins
Recrossing factor calculation			
dt	0.0001	0.0001	Time step (ps)
$t_{\text{equilibration}}$	20	20	Equilibration period (ps) in the constrained (parent) trajectory
$N_{\text{totalchild}}$	200000	200000	Total number of unconstrained (child) trajectories
$t_{\text{childsampling}}$	3	3	Sampling increment along the parent trajectory (ps)
N_{child}	100	100	Number of child trajectories per one initially constrained configuration
t_{child}	2	4	Length of child trajectories (ps)

[a] Detected automatically by RPMDrate.

Table S2: Continuous supersonic flow characteristics.

Laval nozzle	Mach2 Ar	Mach3 Ar	Mach4 Ar
Mach number	2.0 ± 0.03^a	3.0 ± 0.1	3.9 ± 0.1
Carrier gas	Ar	Ar	Ar
Density ($\times 10^{16}$ cm^{-3})	12.6	14.7	25.9
Impact pressure (Torr)	10.5	15.3	29.6
Stagnation pressure (Torr)	13.9	34.9	113
Temperature (K)	127 ± 2^a	75 ± 2	50 ± 1
Mean flow velocity (ms^{-1})	419 ± 3^a	479 ± 3	505 ± 1

[a]The errors on the Mach number, temperature and mean flow velocity, cited at the level of one standard deviation from the mean are calculated from separate measurements of the impact pressure using a Pitot tube as a function of distance from the Laval nozzle and the stagnation pressure within the reservoir.

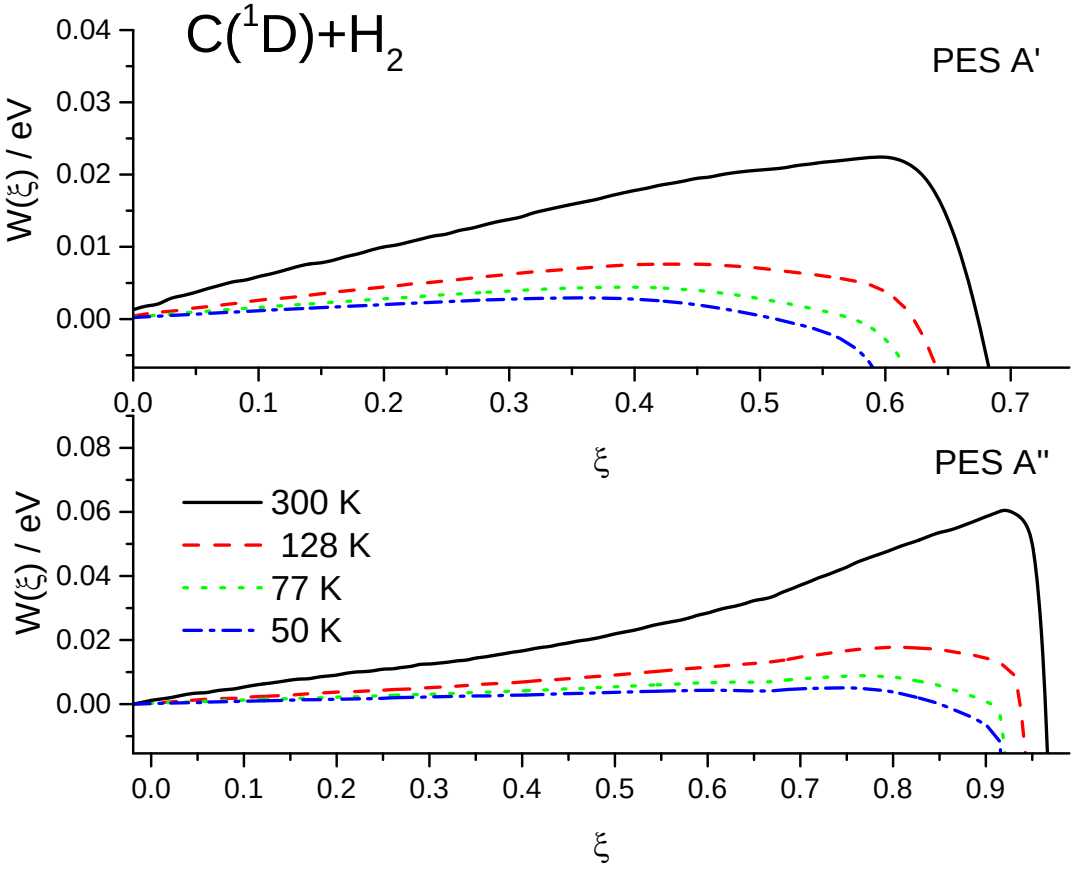

Figure S1: Ring polymer potentials of mean force ($W(\xi)$) along the reaction coordinate for the C(^{1}D) + H_2 chemical reaction on the $^1A'$ (top panel) and $^1A''$ (bottom panel) potential energy surfaces (PESs) at 50, 77, 128 and 300 K. Although both PESs for this reaction have barrierless reaction paths, small free-energy barriers occur prior to the complex (deep well). This is due to the entropic factor and is weakly temperature dependent, as expected [24,25]. While the ring-polymer free energy barrier height is visually higher on the $1A''$ PES, the centroid density k_{QTST} rate coefficients are higher for this PES. One should keep in mind that $W(\xi)$ does not represent an independent characteristic - the k_{QTST} rate coefficients are computed as $\sim R_\infty^2 e^{-\beta(W(\xi)-W(0))}$). For the present calculations, we have chosen $R_\infty = 20$ a_0 for $^1A'$ and 20 Å for $^1A''$ (see Table S1) but verified that the final k_{RPMD} rate coefficients do not depend on R_∞ (provided that this parameter is selected to be large enough).

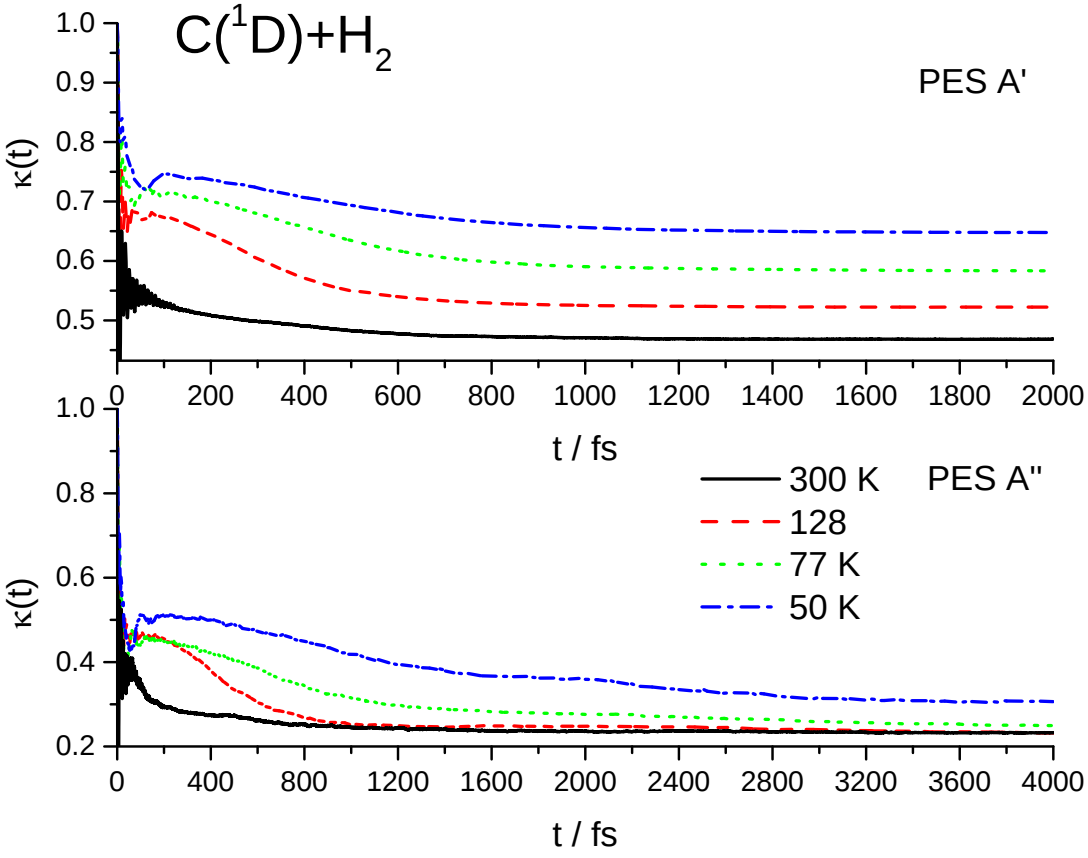

Figure S2: Ring polymer recrossing factors ($\kappa(t)$) along the reaction coordinate for the C(^{1}D) + H_2 chemical reaction on the $^1A'$ (top panel) and $^1A''$ (bottom panel) PESs at 50, 77, 128 and 300 K.

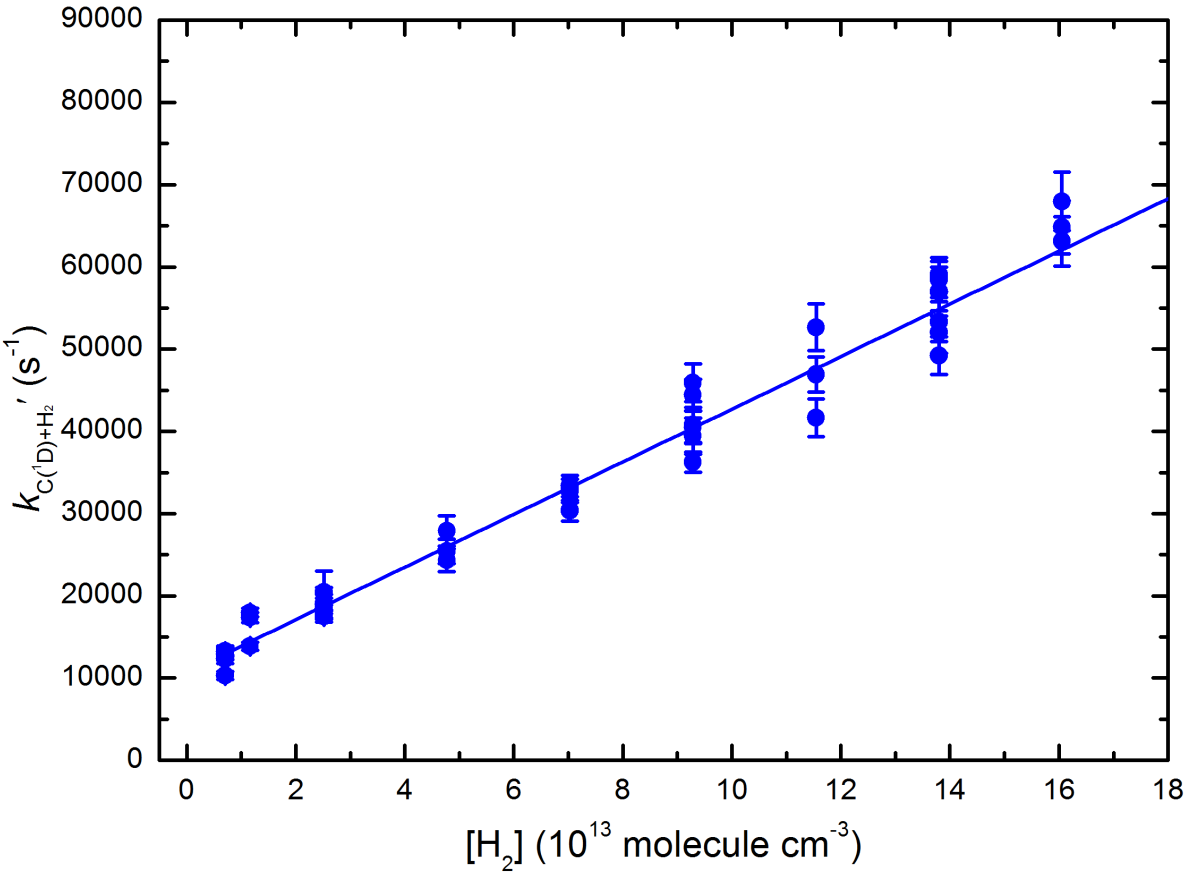

Figure S3: Pseudo-first-order rate coefficients for reaction (1) as a function of [H_2] at 300 K. A weighted linear least-squares fit yields the rate coefficient k_1. The error bars on the ordinate reflect the statistical uncertainties (1σ) obtained by fitting to H atom VUV LIF profiles such as those shown in Figure 1.

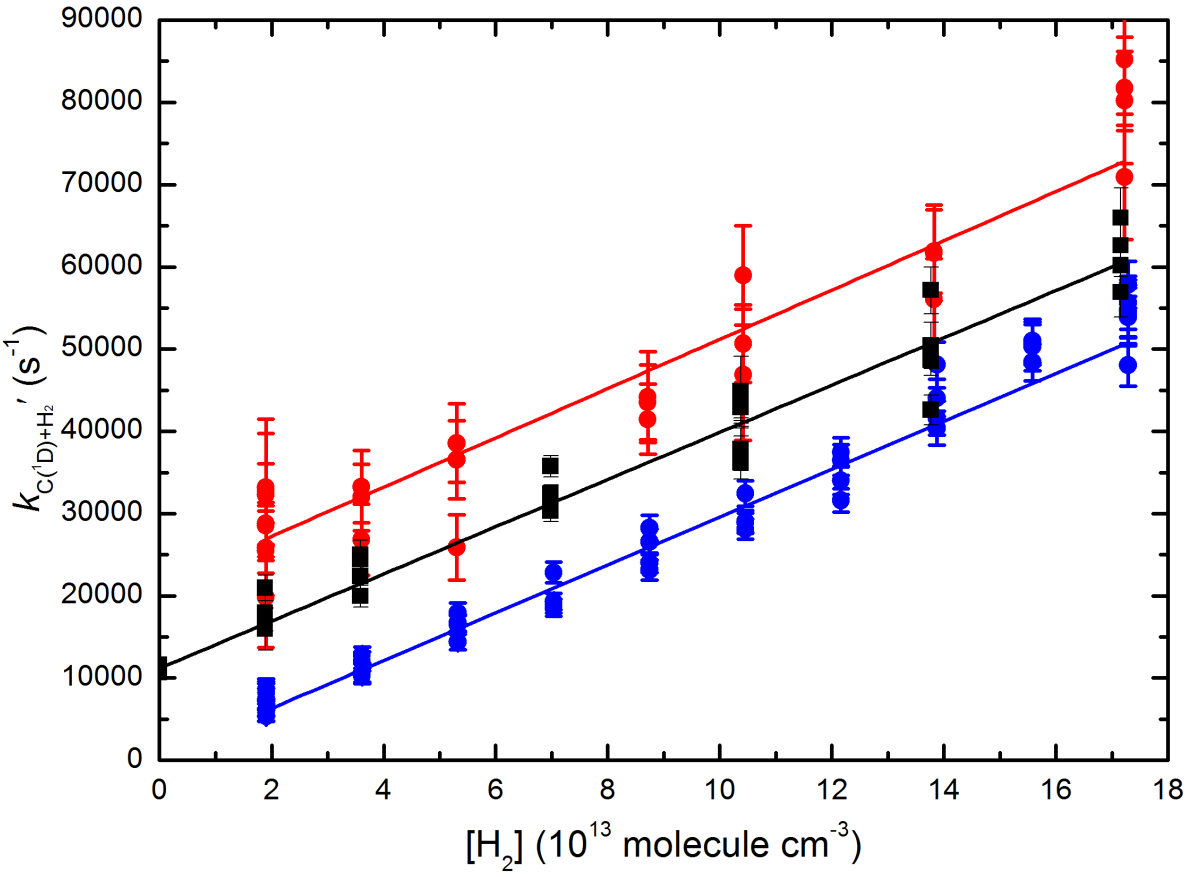

Figure S4: Pseudo-first-order rate coefficients for reaction (1) as a function of [H_2] at 127 K. The red and blue data represent data taken at different [CBr_4]. A weighted linear least-squares fit yields the rate coefficient k_1. The error bars on the ordinate reflect the statistical uncertainties (1σ) obtained by fitting to H atom VUV LIF profiles such as those shown in Figure 1. The black data represent experiments performed using the chemiluminescence detection method outlined in Shannon et al. [54]. The error bars on the ordinate reflect the statistical uncertainties (1σ) obtained by fitting to chemiluminescence decays in a similar manner to Shannon *et al.*

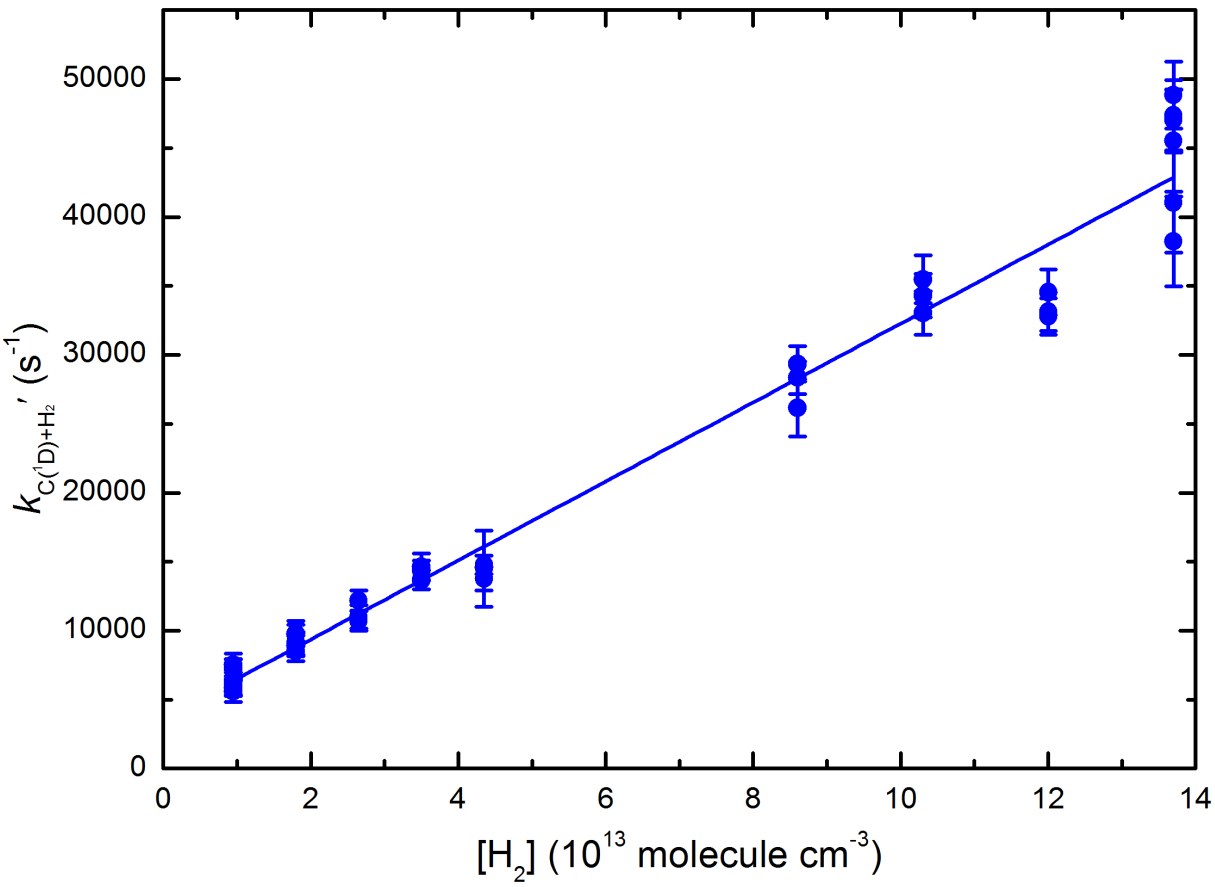

Figure S5: Pseudo-first-order rate coefficients for reaction (1) as a function of [H_2] at 75 K. A weighted linear least-squares fit yields the rate coefficient k_1. The error bars on the ordinate reflect the statistical uncertainties (1σ) obtained by fitting to H atom VUV LIF profiles such as those shown in Figure 1.